Title

Al-doped ZnO aligned nanorod arrays: significant implications for optic and opto-electronic applications

Journal

Journal of Nanophotonics, 6(1)

ISSN

1934-2608

Authors

Holloway, Terence
Dondapati, Hareesh

Publication Date

2012-04-26

DOI

10.1117/1.JNP.6.063507

Peer reviewed

Journal of Nanophotonics

SPIEDigitalLibrary.org/jnp

Al-doped ZnO aligned nanorod arrays: significant implications for optic and opto-electronic applications

Terence Holloway
Rajeh Mundle
Hareesh Dondapati
Messaoud Bahoura
Aswini K. Pradhan

SPIE

Al-doped ZnO aligned nanorod arrays: significant implications for optic and opto-electronic applications

Terence Holloway, Rajeh Mundle, Hareesh Dondapati, Messaoud Bahoura, and Aswini K. Pradhan
Norfolk State University, Center for Materials Research, 700 Park Avenue, Norfolk, Virginia 23504
apradhan@nsu.edu

Abstract. We investigated the optical and optoelectronic properties of vertically aligned Al:ZnO nanorod arrays synthesized by the hydrothermal technique at a considerably low temperature on a sputtered Al:ZnO seed layer. The nanorod arrays maintained remarkable alignment along the c-axis over a large area. The seed layers and nanorod arrays showed various optical band gaps. Investigation of the optoelectronic properties of nanorod arrays on Al:ZnO/p-Si seed layer with SiO_2 revealed that the photocurrent is significantly reduced in nanorod arrays on a AZO/SiO_2/p-Si heterojunction due to multiple scattering phenomena associated with nanorod arrays. This research may open up venues for various optical and opto-electronic applications where highly aligned nanostructures are desired. © *2012 Society of Photo-Optical Instrumentation Engineers (SPIE).* [DOI: 10.1117/1.JNP.6.063507]

Keywords: aligned nanostructures; optical properties; photo-current; semiconductor materials.

Paper 11133 received Nov. 30, 2011; revised manuscript received Mar. 2, 2012; accepted for publication Mar. 12, 2012; published online Apr. 26, 2012.

1 Introduction

Vertically aligned nanorod arrays provide a simple matrix to study the average effect of assembled nanorods.[1–4] One-dimensional (1-D) semiconductor nanomaterials have been attracting attention due to their outstanding properties, which are different from bulk materials. Particularly, well-aligned ZnO nanorod arrays show great potential for solar cell applications.[5,6] Nanorods have been used to increase pn-junction area in dye-sensitized solar cells[7] and in polymer semiconductor hybrid solar cells.[8] High mobility nanorods are pathways for exciton diffusion into pn-junctions in solar cells.[9] The charge transport, as well as tailoring of band gap by either doping or quantum confinement due to size effects, are considered to be very import issues for the application of semiconductor nanostructures, especially for solar cell applications. Furthermore, a template-free (e.g., not using porous alumina template), well aligned growth of nanostructure with micro-structural and optical characteristics of the solution- grown Al-doped ZnO nanorod arrays have significant impact for optical, electronic and, opto-electronic applications. Zinc oxide is a direct n-type semiconductor with a wurtzite hexagonal structure, presenting a wide band gap (3.3 eV at room temperature) and a large exciton binding energy (60 meV). Highly oriented vertical nanorod arrays are highly desired for their future application in various fields such as nanoelectronic or photoelectronic materials where 1-D directionality is needed (e.g., lasing and photonic effects). Also, light scattering properties are under intense focus for application in the field of solar cells in order to enhance the absorption of light in thin absorber layers.

In this paper, we report almost perfect, vertically aligned ZnO nanorod arrays synthesized by the hydrothermal route at 90°C on a sputtered Al:ZnO seed layer. The nanorod arrays demonstrate remarkable alignment along the c-axis over a large area. The optical properties of the seed layers, as well as the nanorod arrays, were investigated. The optoelectronic properties of nanorod arrays on an Al:ZnO/p-Si seed layer with SiO_2 have been illustrated. Our results clearly demonstrate that the photocurrent is significantly reduced in nanorod arrays on an AZO/SiO_2/p-Si heterojunction due to multiple scattering phenomena associated with the nanorod arrays.

0091-3286/2012/$25.00 © 2012 SPIE

However, this can be an opportunity for reabsorption of light by dye or photovoltaic polymers for enhanced effects.

2 Samples Preparation

Al: ZnO (AZO) seed layer films were deposited on boron doped p-Si and glass substrates by radio frequency (RF) sputtering technique using an atmospheric (AR) pressure of 2.2 mTorr, rf power, 150 W, deposition temperature of 350°C, and a deposition time of 20–30 min. An AZO (2 wt% Al_2O_3) ceramic target was used to deposit the Al:ZnO seed layer film. The Si substrate was cleaned using a mixture of $HF:H_2O$ (1:10) in order to remove SiO_2 and achieve H-terminated surface.

AZO nanorod arrays were grown by the hydrothermal method.[8] The AZO seed coated samples were placed in an aqueous solution (50 ml) of different molarity concentrations {0.1 M and 0.05 M zinc nitrate $[Zn(NO_3)_2]$, 0.1 M and 0.05 M hexamethylenetetramine (HMT)} and different wt% (1%, 5%, and 10%) of Al doping. For Al doping, $Al(NO_3)_2$ was used to explore the effect of each chemical on the growth parameters of the nanorod arrays. All precursors were dissolved in deionized water. A glass bottle with the cap screwed on tightly was used and heated in a silicon oil bath at a 95°C, for two to four hours. At the end of the growth period, the samples were cooled to room temperature and removed from the solution. Then, the samples were immediately rinsed with deionized water to remove any residual salt from the surface. Finally, the samples were blown with nitrogen and dried in an oven at 100°C for 10–15 min. It is noted that we report only for concentration, i.e., 5 wt% of Al doping by nitrate precursors.

Thickness measurement of the seed layer was performed using Dektak porofilometer and found to be about 150 nm. The x-ray diffraction (XRD) measurements were performed on a Rigaku powder x-ray diffractometer with Copper Kα incident radiation ($\lambda = 1.5405$Å) to examine the crystallographic structure. X-ray diffraction studies show an intense (002) peak, indicating Wurzite structure. Most of the nanorods grow with their c-axis normal to the surface indicating that the nanorod arrays aligned vertically to the surface of the seed layer. Further examination of the XRD curves revealed a gradual increase in the 100, 002, and 101 peak intensities with an annealing temperature indicating improved crystallinity.

A transmission electron microscope (TEM) was used to determine the crystal structure and morphology. A field emission-scanning electron microscope (FE-SEM), Hitachi 4700 scanning electron microscope, and JEOL JSM-5900LV scanning electron microscope (SEM) were used to examine the surface morphology and orientation of the nanorods arrays. The atomic force microscopy (AFM) study of the surface roughness and surface grain size of ZnO seed layers was performed using a Bruker dimension Icon AFM microscope. The absorption was measured by UV-VIS-IR spectrophotometer (Perkin Elmer Lambda 950 UV-VIS-IR). The optical absorption was measured against bare glass as a reference to obtain the absorption of the AZO seed layer. Air and an AZO seed layer were used as a reference sample to obtain absorption of the AZO nanorod arrays. Temperature dependence of the electrical resistivity was measured using a four-probe technique. The photocurrent was measured from the current-voltage characteristics using a solar simulator.

3 Results and Discussion

Figure 1 shows the typical FE-SEM and AFM images of the seed layers. The SEM image [Fig. 1(a)] of the seed layer clearly illustrates that the grains are very uniform in size. The grain size is typically 30 nm in size. This is being confirmed by the AFM image shown in Fig. 1(b). The surface roughness is about 1 nm. The films are optically very smooth without having any microscopic defects. The major merit of using the seed layer is to nucleate and guide the nanorod growth in an array form. On the other hand, it provides a template free growth opportunity with electrical contact and optical transparency of the seed layer because AZO is a transparent conducting oxide (TCO).

Figure 2(a)–2(c) shows the SEM images of Al:ZnO nanorod arrays with 5 wt% of Al in ZnO. Typically the nanorod dimensions are the following: length $\sim 1\ \mu m$, diameter $\sim 70\ to\ 80\ nm$, and nanorod density $\sim 3.2 \times 10^9$ rods/cm^2, calculated from the selected area of a FE-SEM image.

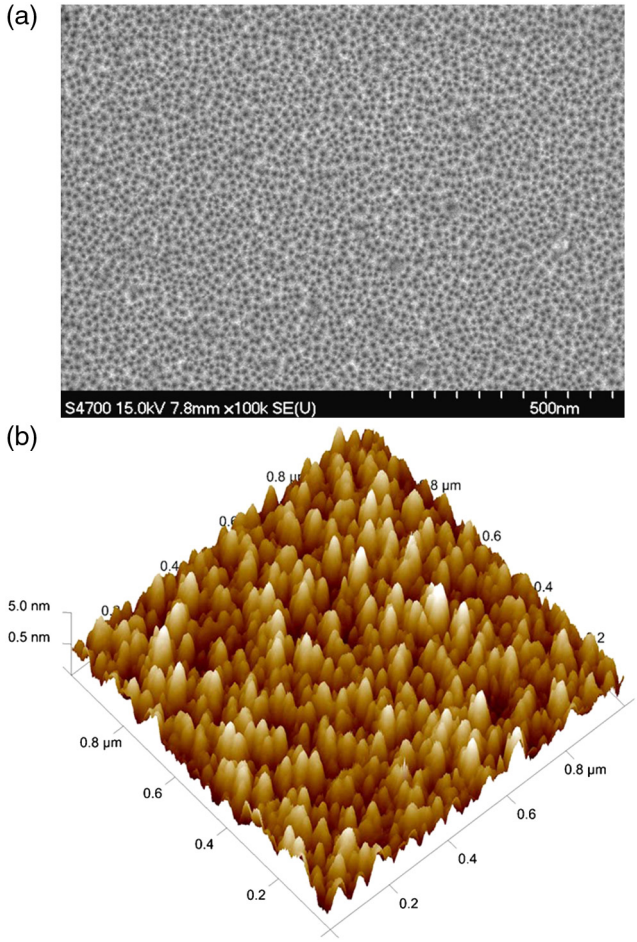

Fig. 1 (a) FE-SEM image of Al:ZnO seed layer and (b) is AFM image of the seed layer ($1 \times 1\ \mu m^2$).

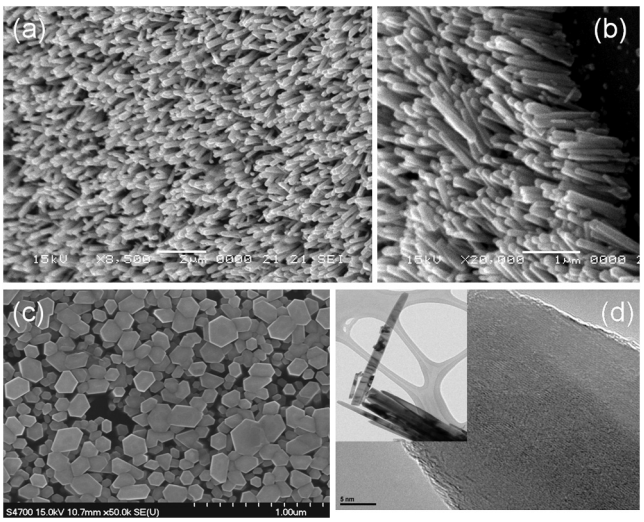

Fig. 2 (a) SEM image of Al:ZnO nanorod array, (b) tilt angle view of the nanorod array, (c) top view of the nanorods, and (d) TEM image of the nanorod in the inset shown. 5 wt% aluminum is used in the growth solution.

However, there are some nanorods with diameters below 40 nm. Figure 2 shows the top (a) as well as 45 deg tilt angle (b) views of the nanorod array. Nanorods grow normal to the surface. The nanorods present a nanopillar shape, and they represent a hexagonal shape from the top. It is observed that at some point the longitudinal growth is stopped close to 1 μm, which is very unique when Al:ZnO seed layer is used, and has been observed by other authors.[9] The nanorods present a nanopillar shape and represent a hexagonal shape from the top. It is observed that at some point the longitudinal growth is stopped close to 1 μm, which is very unique when an Al:ZnO seed layer is used. The average length of the nanorod is around 1 μm for the current growth time. This is mainly due to the fact that the nucleation centers are first formed on the homostructure of an AZO seed layer film. Once the nucleation initiates on a few grains, forming a hexagonal base as shown in Fig. 2(c), the density of nanorods remains rather constant after the initial nucleation stage. The TEM image [Fig. 2(d)] also demonstrates that ZnO is crystalline for the AZO nanorod shown in the inset of Fig. 2(d). It is also noted that the energy dispersive spectroscopy (EDS) study of AZO nanorods show Al concentration of about 3%, which is slightly more than the Al concentration (~2.6%) measured using x-ray photoelectron spectroscopy.

Figure 3 shows the temperature-dependent resistivity curves measured using a four-probe electrode configuration in order to compare the resistivity of Al:ZnO on glass and p-Si substrates grown at 350°C. The lower resistivity of the Al:ZnO/glass films grown can be explained due to the Burstein-Moss effect,[10] in which Fermi level shifts to the conduction band of a degenerate semiconductor leads to an energy band widening and is consistent with our optical data. The metal-like and metal–semiconductor transition behavior was observed to have a metal–semiconductor transition (MST) in the vicinity of 125 K to 130 K for the current films. However, the resistivity continued decreasing to $T = 100$ K, showing a characteristic up-turn in resistivity behavior at low temperature which is generally found in an impure metal. The film showed a positive temperature coefficient of resistance (TCR) above MST and a negative TCR below it as we reported earlier.[11] The lower resistivity of ZnO/glass than that of ZnO/p-Si can be attributed to the defects which is evident from the higher residual resistivity in ZnO/p-Si. One of the possible reasons is due to the interfacial defects between Si and Al:ZnO film.

Figure 4 shows the optical absorption spectra of AZO films on glass substrates. The absorption edge of AZO/glass shifts to a higher wavelength for nanorod arrays grown on AZO seed layer. The absorption edge of AZO/glass film shifts to a lower wavelength indicating an increase in band gap opposite to the nanorod arrays. The transmission of AZO film shows a dramatic reduction from 90% to below 40% for nanorod arrays on an AZO seed layer (see inset of Fig. 4). The reason for this reduction can be related to the enhanced diffusion in the visible wavelength

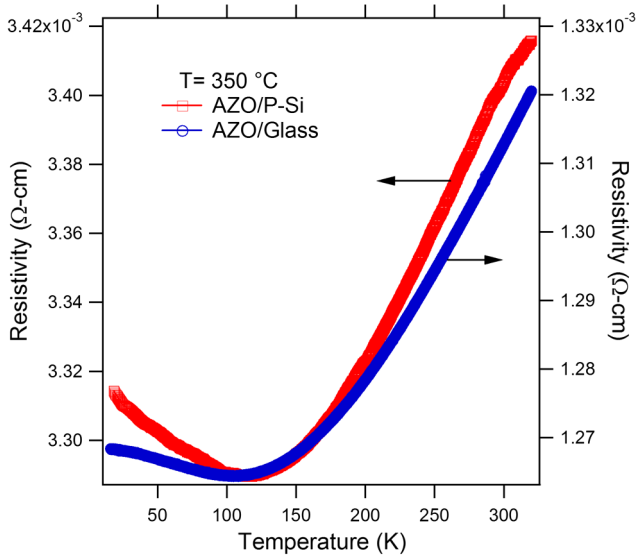

Fig. 3 Temperature dependence of electrical resistivity of Al:ZnO seed layers on glass and P-Si substrates.

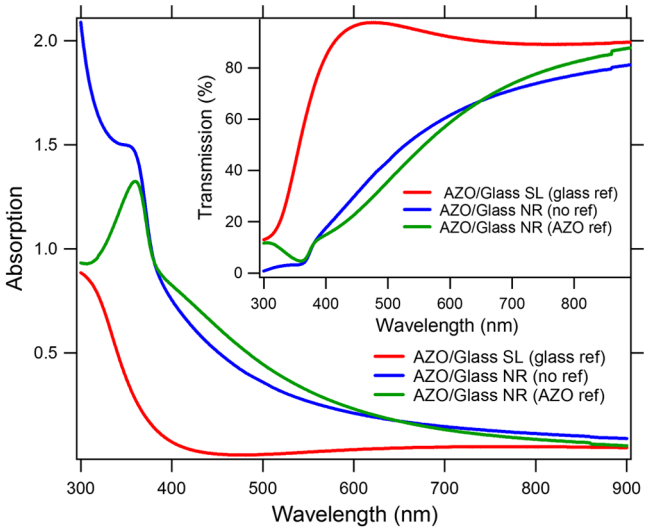

Fig. 4 Absorption spectra of the AZO/glass substrate and nanorods grown on AZO/glass substrates with and without nanorods grown on the surface. AZO/glass is used as a reference substrate. The inset shows the transmission spectra of AZO/glass substrate and nanorods grown on AZO/glass substrates with and without nanorods.

region and the trapping of light in the nanorod arrays which explains their enhanced absorption. The measurement of absorption is not absolute since the presence of diffusion will appear as an additional loss from the ballistic contribution. Hence the total absorption measurement is essential. The antireflecting[12] and scattering effects of vertically oriented nanorod arrays with higher surface densities are the major reasons for nanorod arrays' reduced transmission. Each nanorod acts as a scattering center[13] and enhances the multiple scattering for a certain range of wavelengths due to nanorod arrays. This causes a significant drop in the total transmission from 90% to below 40% as observed in the present case, and the layer is fairly transparent. The scattering of light is very intense when the light falls on the samples with nanorods as opposed to the AZO/glass seed layer.

In a high absorption region, Tauc,[14] and Davis and Mott[15] showed that the absorption coefficient and photon energy are related by the following equation.

$$\alpha \mathrm{hv} = A(\mathrm{hv} - E_g)^n. \tag{1}$$

In the above equation, A is a constant, E_g is the band gap of the material, and n has different values depending on the optical absorption process. It was found that $n = 1/2$ is the best fit for our results and is characteristic of the direct band absorption without phonon mediation. Figure 5 shows the $(\alpha \mathrm{hv})^2$ versus hv plot from which the optical band gap was determined. It is very clear that the band gap for the nanorod arrays/AZO/glass is ~3.18 eV, while the band gap for the AZO/glass seed layer is 3.5 eV. It is noted that the band gap for ZnO film is 3.33 eV. The blue shift of the band gap for nanorod arrays/AZO/glass can be explained due to the effect of quantum confinement, while the red shift of the band gap for AZO/glass seed layer is attributed to Al doping. The peak at ~360 nm (~3.44 eV) in samples containing AZO nanorod arrays may be contributed to Al doping. However, the diameter of nanorods prepared in this work is larger than that required for the quantum confinement. One of the possible reasons is that the diameter of some of the nanorods may be smaller in size as seen in Fig. 2(c) (tops of the nanorods, typically less than 40 nm). However, the reason for the blue-shift of the band gap at 3.18 eV requires further investigation.

Al:ZnO film is highly transparent ($T > 90\%$) in the visible region which allows the visible light to pass through the AZO film. For AZO/p-Si, the light is primarily absorbed in the underlying p-Si. This generates electron–hole pairs, producing the photocurrent under reverse bias conditions. As the UV photons are mainly absorbed in the AZO layer, the photo-generated electrons are drifted towards the positive electrode through the AZO region. This gives rise

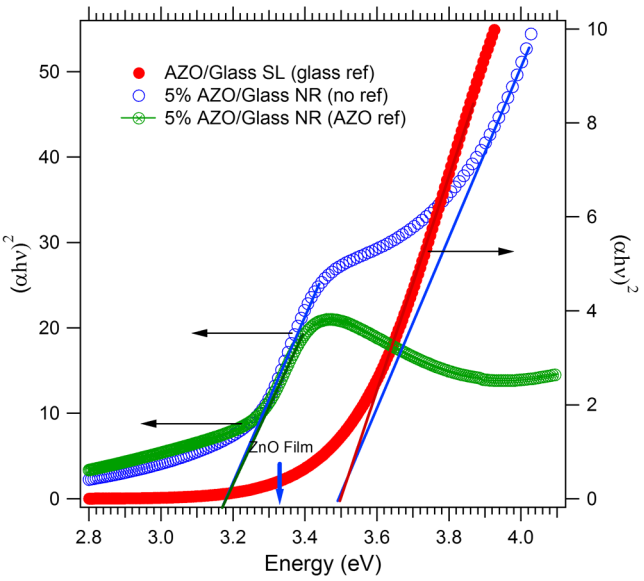

Fig. 5 Optical band gap of AZO/glass with and without nanorod arrays. Glass as well as AZO references were used to distinguish the nanorod contribution.

to the increase in current almost linearly as the reverse bias increases (not shown here). On the other hand, the p-type silicon surface provides a supply of electrons which can enter into the AZO film. The effective coupling current flows due to the interchange of the charge between the conduction and valence bands of the silicon by recombination-generation. However, due to a linear increase in current with increasing reverse bias, the diode characteristic did not arise. In order to see this effect, the $AZO/SiO_2/p\text{-}Si$ heterojunction was fabricated in which SiO_2 works as an insulating barrier. This junction was illuminated under the halogen lamp with 1 $Watt/cm^2$ in order to observe the photovoltaic effect. The nanorods were grown on $AZO/SiO_2/p\text{-}Si$ heterojunction. Figure 6 shows the current density versus bias voltage for $AZO/SiO_2/p\text{-}Si$ heterojunction with and without nanorods on the surface of the AZO seed layer.

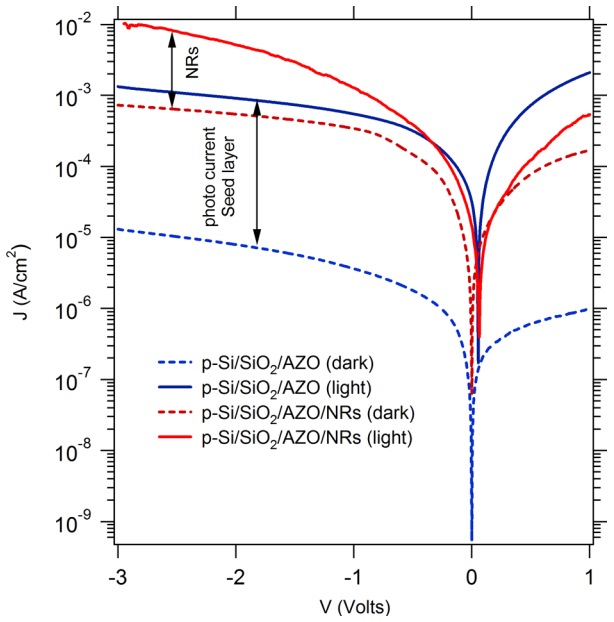

Fig. 6 Current density versus voltage characteristics of the seed layer and seed layer with nanorods. SiO_2 barrier layer is used to inhibit channeling of the current.

The insulating barrier worked to increase the depletion region between AZO and p-Si. It is remarkable that the photo-current is reduced significantly in samples with nanorods. As discussed earlier, the scattering effects of highly vertically oriented nanorod arrays with higher surface densities are responsible for the reduced transmission for nanorod arrays and reduced absorption by the seed layer. However, it is anticipated that the similar structure of nanorod arrays will enhance the photo-current when dye-sensitized.[16,17] This is due to the reabsorption of light in the dye due to multiple scattering phenomena by the nanorods.

4 Conclusions

In summary, we report the optical and optoelectronic properties of vertically aligned Al:ZnO nanorod arrays synthesized by the hydrothermal technique at a considerably low temperature on a sputtered Al:ZnO seed layer. The morphology demonstrates that the nanorod arrays maintain remarkable alignment along the c-axis over a large area. The investigation of the optical properties of the seed layers as well as the nanorod arrays show varied band gaps. The optoelectronic properties of nanorod arrays on an AZO/SiO_2/p-Si heterojunction with a SiO_2 barrier ayer have been illustrated. The photocurrent is significantly reduced in nanorod arrays on an AZO/SiO_2/p-Si heterojunction due to multiple scattering phenomena associated with the nanorod arrays. This research may open up venues for various optical and opto-electronic applications where highly aligned nanostructures are desired.

Acknowledgments

This work is supported by the DoD (CEAND) Grant Number W911NF-11-1-0209 (US Army Research Office), NSF-CREST (CNBMD) Grant Number HRD 1036494, and NSF-RISE-HRD-0931373. The authors are thankful to R.B. Konda for experimental help. All authors have equal contribution.

References

1. C. J. Lee et al., "Field emission from well-aligned zinc oxide nanowires grown at low temperature," *Appl. Phys. Lett.* **81**(19), 3648–3650 (2002), http://dx.doi.org/10.1063/1.1518810.
2. W. I. Park and G. C. Yi, "Electroluminescence in n-ZnO nanorod arrays vertically grown on p-GaN," *Adv. Mater.* **16**(1), 87–90 (2004), http://dx.doi.org/10.1002/adma.200305729.
3. L. Vayssieres et al., "Purpose-Built anisotropic metal oxide material: 3d highly oriented microrod array of ZnO," *J. Phys. Chem. B* **105**(17), 3350–3352 (2001), http://dx.doi.org/10.1021/jp010026s.
4. L. Vayssieres, "Growth of arrayed nanorods and nanowires of ZnO from aqueous solutions," *Adv. Mater.* **15**(5), 464–466 (2003), http://dx.doi.org/10.1002/adma.200390108.
5. D. C. Olson et al., "Hybridphotovoltaic devices of polymer and ZnO nanofiber composites," *Thin Solid Films* **496**(1), 26–29 (2006).
6. K. Takanezawa et al.," Efficient charge collection with ZnO nanorod array in hybrid photovoltaic devices," *J. Phys. Chem. C* **111**(19), 7218–7223 (2007).
7. B. O'Regan and M. Grätzel, "A low-cost, high-efficiency solar cell based on dye-sensitized colloidal TiO_2 films," *Nature* **353**(6346), 737–740 (1991).
8. S. Yun et al., "Hydrothermal synthesis of Al-doped ZnO nanorod arrays on Si substrate," *Phys. B: Condense Matter* **405**(1), 413–419 (2010).
9. S. Baruah and J. Dutta, "Hydrothermal synthesis of Al-doped ZnO nanorod arrays on Si substrate," *J. Cryst. Growth* **311**(8), 2549–2554 (2009), http://dx.doi.org/10.1016/j.jcrysgro.2009.01.135.
10. E. Burstein, "Anomalous optical absorption limit in InSb," *Phys. Rev.* **93**(3), 632–633 (1954), http://dx.doi.org/10.1103/PhysRev.93.632.
11. C. Fournier et al., "Effects of substrate temperature on the optical and electrical properties of Al:ZnO films," *Semicond. Sci. Technol.* **23**, 085019 (2008), http://iopscience.iop.org/0268-1242/23/8/085019

12. Y.-J. Lee et al., "ZnO nanostructures as efficient antireflection layers for solar cells," *Nano Lett.* **8**(5), 1501–1505 (2008).
13. R. Tena-Zaera, J. Elias, and C. Levy-Clement, "ZnO nanowire arrays: optical scattering and sensitization to solar light," *Appl. Phys. Lett.* **93**(23), 233119–233121 (2008), http://dx.doi.org/10.1063/1.3040054
14. J. Tauc, *Optical Properties of Solids* **22**, F.Abeles, Ed., North Holland Pub, Amsterdam, (1970).
15. E. A. Davis and N. F. Mott, "Conduction in non-crystalline systems *v*. conductivity, optical absorption and photoconductivity in amorphous semiconductors," *Philos. Mag.* **22**(179), 903–922 (1970).
16. Y. Y. Lin et al., "Nanostructured metal oxide/conjugated polymer hybrid solar cells by low temperature solution processes," *J. Mater. Chem.* **17**(43), 4571–4576 (2007), http://dx.doi.org/10.1039/b710400f
17. G.-C. Yi, C. Wang, and W. I. Park, "ZnO nanorods: synthesis, characterization and applications," *Semicond. Sci. Technol.* **20**, S22–S34 (2005), http://dx.doi.org/10.1088/0268-1242/20/4/003

Biographies and photographs of the authors are not available.